



# 1 **A conceptual model for glacial lake bathymetric distribution**

2 **Taigang Zhang<sup>1,2,3</sup>, Weicai Wang<sup>2</sup>, Baosheng An<sup>2,4</sup>**

3 <sup>1</sup>College of Earth and Environmental Sciences, Lanzhou University, Lanzhou 730000, China

4 <sup>2</sup>State Key Laboratory of Tibetan Plateau Earth System, Environment and Resources (TPESER), Institute of Tibetan  
5 Plateau Research, Chinese Academy of Sciences, Beijing 100101, China

6 <sup>3</sup>Center for the Pan-Third Pole Environment, Lanzhou University, Lanzhou 730000, China

7 <sup>4</sup>School of Science, Tibet University, Lhasa 850011, China

8

9 **Correspondence:** Taigang Zhang (zhangtg16@lzu.edu.cn) and Weicai Wang (weicaiwang@itpcas.ac.cn)

10

11 **Abstract.** The formation and expansion of glacial lakes worldwide due to global warming and  
12 glacier retreat have been well documented in the past few decades. Thousands of glacial lake  
13 outburst floods (GLOFs) originating from moraine-dammed and ice-dammed lakes were reported,  
14 causing devastating impacts on downstream lives and properties. Detailed glacial lake bathymetry  
15 surveys are essential for accurate GLOF simulation and risk assessment. However, these bathymetry  
16 surveys are still scarce as glacial lakes located in remote and high-altitude environments hamper a  
17 comprehensive investigation. We developed a conceptual model for glacial lake bathymetric  
18 distribution using a semi-automatic simulation procedure. The basic idea is that the statistical glacial  
19 lake volume-area curves conform to a power-law relationship indicating that the idealized geometric  
20 shape of the glacial lake basin should be hemispheres or cones. First, by reviewing the evolution of  
21 various types of glacial lakes, we identified 10 standard conceptual models to describe the shape of



22 lake basins. Second, we defined a general conceptual model to depict the continuum transitions  
23 between different standard conceptual models for those specific glacial lakes that lie between two  
24 standard conceptual models. Third, we nested the conceptual model into the actual glacial lake basin  
25 to construct the water depth contours and interpolate the glacial lake bathymetric distribution. We  
26 applied the conceptual model to simulate three typical glacial lakes in the Tibetan Plateau with in-  
27 situ bathymetric surveys to verify the algorithm's applicability. The results show a high consistency  
28 in the point-to-point comparisons of the measured and simulated water depths with a total volume  
29 difference of approximately  $\pm 10\%$ . The conceptual model has significant implications for  
30 understanding glacial lake evolution and modeling GLOFs in the future.

31

## 32 **1 Introduction**

33 Globally, glacial recession and thinning have been well-documented over the last decades via  
34 field observations and remote sensing techniques (Yao et al., 2012; Zemp et al., 2019; Hugonnet et  
35 al., 2021). Such evolution of glaciers due to climate warming and anthropogenic factors could  
36 induce related effects (Yao et al., 2019), among which is the expansion and formation of glacial  
37 lakes (Zhang et al., 2015; Emmer et al., 2016; Wang et al., 2020; Ma et al., 2021). Glacial lakes are  
38 water bodies developed within depressions of glacier moraine or mainly fed by contemporary  
39 glacier meltwater (Yao et al., 2018). Due to glacier retreats, they are generally impounded by glacier  
40 terminal or lateral moraine. Since the 1990s, the glacial lakes worldwide have increased by around  
41 50% in total number, area, and volume (Shugar et al., 2020), manifesting an ongoing climate change.  
42 These changes have also been accompanied by glacial lake outburst flood (GLOF) risks.



43 As a glacier-related hazard, GLOF has been a frequent incidence in various glacierized areas,  
44 causing considerable socioeconomic losses (Anaconda et al., 2015a; Nie et al., 2018). According to  
45 a compilation by Carrivick and Tweed (2016), approximately 1000 GLOFs from moraine- and ice-  
46 dammed lakes are recorded worldwide and claim more than 10000 deaths. Under the triggering  
47 factors such as ice avalanches, landslides, and heavy precipitation, glacial lakes are extremely  
48 unstable and subsequently cause a sudden release of water with peak discharge higher than a dozen  
49 times that of monsoon rainfall floods (Richardson and Reynolds, 2000; Westoby et al., 2014;  
50 Kougkoulos et al., 2018). However, due to the relatively small volume of the glacial lake, the  
51 flooding process generally proceeds rapidly within a few hours. Knowledge of glacial lake volume  
52 is critical, as it influences the released water volume and GLOFs magnitude (Fujita et al., 2013).  
53 Therefore, lake volume is often employed as an essential criterion in numerous cases of GLOF  
54 susceptibility and risk assessment (Bolch et al., 2011; Aggarwal et al., 2017; Drenkhan et al., 2019;  
55 Falatkova et al., 2019).

56 Currently, only sporadic bathymetric surveys on glacial lakes have been conducted worldwide.  
57 In Cordillera Blanca, Peru, facing continuous threats by GLOFs (Lliboutry et al., 1977), more than  
58 100 detailed bathymetric surveys of glacial lakes have been carried out to understand better the  
59 regional GLOF risks (Muñoz et al., 2020). Government agencies and research institutions have  
60 promoted these surveys. In the Tibetan Plateau and its surroundings, the bathymetric surveys are  
61 focused on the glacial lakes in the Himalayas (Sharma et al., 2018; Watson et al., 2018), where  
62 approximately 60 bathymetric surveys of glacial lakes, such as the Cirenmaco, Jialongco, and  
63 Longbasaba Lake, were conducted (Yao et al., 2012; Wang et al., 2018; Li et al., 2021). They  
64 measure the water depth with ultrasonic devices onboard automatic uncrewed boats or manual



65 hovercrafts.

66 Performing a universal investigation campaign of lake bathymetry is impractical for thousands  
67 of glacial lakes in remote areas and high elevations. Instead, scholars typically utilize single total  
68 lake volume data rather than bathymetric distribution in GLOF modeling (Anaconda et al., 2015b;  
69 Zhang et al., 2021). The lake volume is typically estimated by empirical equation, e.g., direct  
70 volume–area equation (O'Connor et al., 2001; Huggel et al., 2002; Loriaux and Casassa, 2013), or  
71 indirect area–mean depth/maximum depth/width equation (Wang et al., 2012), which have  
72 considerable uncertainty. There is no doubt that the measured and/or interpolated glacial lake  
73 bathymetric distribution have great merit that can precisely determine the maximum potential  
74 outburst volume of the glacial lake, serving to further simulate the GLOF propagation and evaluate  
75 downstream exposures (Frey et al., 2018; Sattar et al., 2021). Moreover, a bathymetry survey is also  
76 pivotal to understanding the interactions between the glaciers and their terminating lakes, as several  
77 studies have revealed that the proglacial lake bathymetric state can dominate the glacier terminal  
78 melting and calving regimes (Sugiyama et al., 2021).

79 Can we obtain glacial lake bathymetric distributions through modeling rather than in situ  
80 investigations? Previous studies have provided insights. Cook and Quincey (2015) preliminarily  
81 proposed that the same type of glacial lakes may have their idealized geometric shapes, which depict  
82 the evolution of glacial lakes' volume–area ( $V-A$ ) relationship over time. For instance, the triangular  
83 cone is suitable to represent the idealized geometric shape of ice-dammed lakes dammed by glaciers  
84 and formed in the narrow valley. The idealized conceptual models of glacial lakes can be combined  
85 with the actual situations to project the glacial lake bathymetric distribution.



86 An idealized lake basin is also helpful in constructing numerical or physical models. In the  
87 study of Veh et al. (2020), the conceptual model of glacial lakes was constructed as a semi-ellipsoid  
88 with a circular surface to calculate the released volume after the lake drainage. The surface area and  
89 height of the semi-ellipsoid refer to the glacier lake area and maximum water depth, respectively.  
90 Based on these instructive designs, we attempted to develop a procedure and algorithm for modeling  
91 glacial lake bathymetric distribution in this study. We first (i) retrieved as many as possible  
92 conceptual models for various types of glacial lakes by reviewing the evolutions of glacial lakes and  
93 analyzing the relationships between lake volumes and areas; (ii) explored the procedure and  
94 algorithm to estimate bathymetric distribution in conjunction with actual lake surface and basin  
95 shapes; and then (iii) discussed their implications and potential applications.

## 96 **2 Data and methods**

### 97 **2.1 Compilation of glacial lake bathymetry**

98 Analyzing the existing glacial lake bathymetries can help us reveal glacial lake water depth  
99 characteristics. To our knowledge, more than 60 articles have mentioned surveyed bathymetry data  
100 from glacial lakes. We integrated the prior studies and established an inventory of global glacial lake  
101 bathymetry (Supplementary material 1). The attributes included the name, location, survey time,  
102 area, volume, and maximum water depth. A total of 231 bathymetric data from 220 glacial lakes  
103 globally were compiled in the inventory (Fig. 1a).

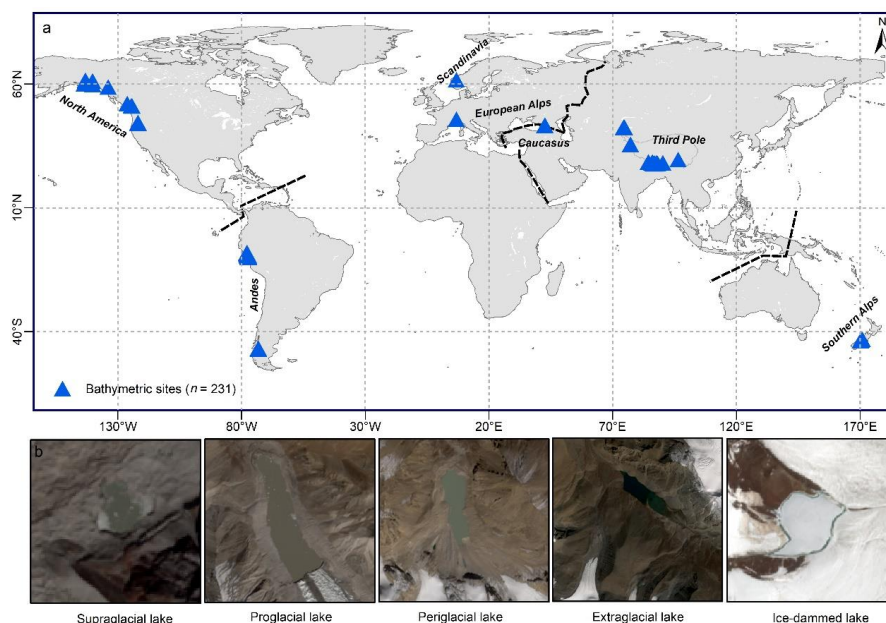
### 104 **2.2 Classification and evolution of different glacial lake types**

105 The maximum water depth ( $D$ ) and total volume ( $V$ ) are the fundamental parameters regarding  
106 the idealized geometric shape of glacial lakes. We used the compiled glacial lake bathymetry data



107 to fit the curves of  $V-A$  (glacial lake area) and  $D-A$  to understand the evolution of glacial lakes and  
108 to develop a conceptual model suitable for describing the shape of an idealized lake basin. We  
109 assumed that different types of glacial lakes have different expansion mechanisms and, thus,  
110 different conceptual models. Based on the topological positions between the glacial lakes and their  
111 parent glaciers, we classified glacial lakes as supraglacial proglacial, periglacial, extraglacial, and  
112 ice-dammed types (Fig. 1b).

113 This classification system considers glaciers' critical role in the evolution of glacial lakes  
114 (Petrov et al., 2017). As for the supraglacial lakes, expansion proceeds in all directions, and the  
115 temperature difference at the ice-water interface continuously melts the glacier ice in both horizontal  
116 and vertical orientations. The proglacial lake's expansion mainly proceeds backward by glacial  
117 retreat. The periglacial lake and the extraglacial lake are not directly in contact with the glacier, and  
118 their expansion depends more on changes in precipitation and glacier meltwater. These various  
119 mechanisms in glacial lake expansions showed that the changes in the lake basin among the different  
120 glacial lake types are inconsistent, indicating that they may have different conceptual models.



121

122 **Figure 1.** (a) Distribution of glacial lakes whose volume was surveyed in detail. (b) Glacial lakes were divided into  
123 five categories, namely proglacial (direct in contact with glacier terminus), periglacial (separated from the glacier  
124 and dammed by historical moraine), extraglacial (far from the glacier and generally dammed by landslides),  
125 supraglacial (positioned on the glacier surface), and ice-dammed lake.

126

### 127 2.3 Standard conceptual model

128 The basic procedure of constructing glacial lake bathymetric distribution is to (i) identify the  
129 most appropriate conceptual model that can describe the idealized lake basin, (ii) calculate the  
130 theoretical formulation equations of this conceptual model, (iii) nest this conceptual model into the  
131 actual glacial lake basin to construct the water depth contours, and (iv) interpolate and calculate the  
132 glacial lake bathymetric distribution. The conceptual model was constructed as the scheme  
133 presented by Veh et al. (2020). Glacial lakes were assumed to have hemispherical or similar three-



134 dimensional lake basin shapes. The standard surface of the glacial lake was assumed to be an ellipse.

135 The general formula between the volume and area of glacial lakes fits a power-law relationship  
136 (Table 1). It could be expressed as Eq. (1). The best-fit curve for the relationship between maximum  
137 water depth and area of glacial lakes also follows the power-law relationship (Eq. 2) (Fig. 2).

138 
$$V = \alpha A^\beta \quad (1)$$

139 
$$D = \gamma A^\varepsilon \quad (2)$$

140 A is the area of the glacial lake;  $\alpha$ ,  $\gamma$ ,  $\beta$ , and  $\varepsilon$  are the coefficients. The value of  $\beta$  is greater  
141 than 1, and  $\varepsilon$  is less than 1.

142 The three-dimensional bodies representing the standard shape of a lake basin were required to  
143 have a general formula as defined by Eq. (3):

144 
$$V = \delta AD \quad (3)$$

145 Here,  $\delta$  is the coefficient, A is the elliptical surface area, and D corresponds to the maximum  
146 water depth of the glacial lake. We identified four hemispheres or cones whose volumes can be  
147 expressed by Eq. (3): the hemisphere structured by the elliptical side ( $V = 2/3AD$ ); the hemisphere  
148 structured by the upward-opening parabolic side ( $V = 1/2AD$ ); the cone structured by the straight  
149 side ( $V = 1/3AD$ ); and the cone structured by the rightward-opening parabolic side ( $V = 1/5AD$ ).  
150 These bodies are defined as the standard conceptual model (SCM), and their curves in the X-O-Z  
151 quadrant are called the standard curves (Fig. 3a). These four standard curves are progressively  
152 concave inward in the quadrant, from the elliptical curve to the rightward-opening parabolic curve.

153 The SCMs for the supraglacial, periglacial, and extraglacial lake types are compatible with the





154 expansion mechanisms partly because their growth direction is comprehensive at the horizontal  
155 level. However, proglacial lakes are different. Their expansions are focused toward the glacier's  
156 direction, and the maximum water depths are situated near the intersection with the glacier. Under  
157 these circumstances, we considered the SCMs of proglacial lakes to be half of the preceding four  
158 SCMs, such as the semi-cone structured by the straight side. We also took into account the way in  
159 which the SCMs of the ice-dammed lake formed. We ultimately designed two SCMs: the semi-cone  
160 structured by the straight side and the triangular cone ( $V = 1/3AD$ ). Most of the actual volume points  
161 lie between the volume curves of these SCMs (Fig. 4), and there are one or two closer SCM volume  
162 curves for each type of glacial lake's fitted A–V curve.

163

164 **Table 1.** Empirical equations of volume and area of glacial lakes in previous studies. The applicable region, lake  
165 type, and sample size for each empirical equation were indicated during fitting. The unit volume is  $10^6 \text{ m}^3$ , and the  
166 area unit is  $\text{km}^2$ .

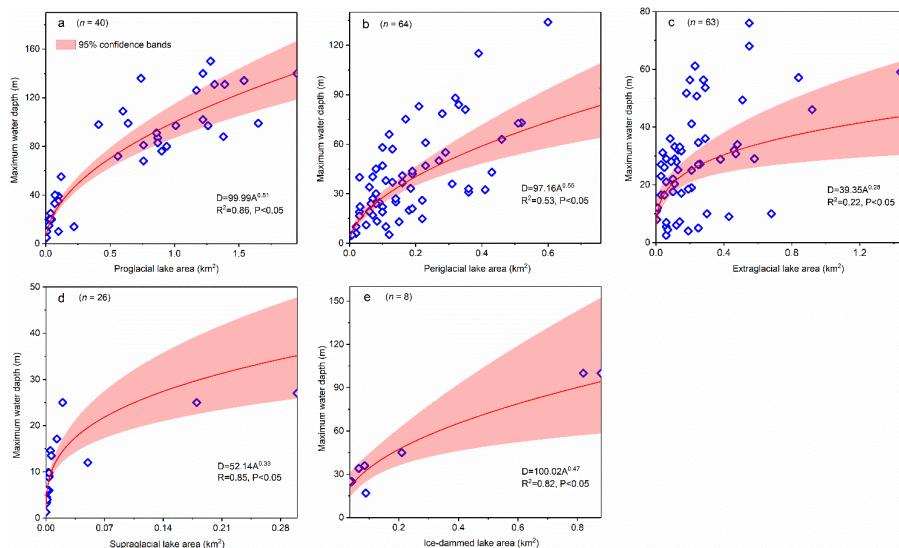
ID	Empirical formulas	Region	Lake types	Samples	Reference
1	$V = 35A^{1.5}$	British Columbia, Canada	Ice-dammed lake	not mentioned	Evans, 1986
2	$V = 168.5A^2 + 3.11A$	Northwestern America	Moraine-dammed lake	7	O'Connor et al., 2001
3	$V = 34.44A^{1.42}$	Worldwide	Moraine- and ice-dammed lake	13	Huggel et al., 2002
4	$V = 43.24A^{1.53}$	Himalayas	Moraine-dammed lake	17	Sakai, 2012
5	$V = 6.07A^{1.37}$	Himalayas	Moraine-dammed lake	20	Wang et al., 2012
6	$V = 55A^{1.25}$	Himalayas	Moraine-dammed lake	20	Fujita et al., 2013
7	$V = 33.58A^{1.39}$	Worldwide	Moraine- and ice-dammed lake	31	Loriaux and Casassa, 2013



8	$V = 42.93A^{1.48}$	Peruvian Andes	Moraine- and bedrock-dammed lake	35	Emmer and Vilímek, 2014
9	$V = 34.07A^{1.37}$	Worldwide	Various types	69	Cook and Quincey, 2015
10	$V = 11.49A^{1.26}$	Worldwide	Supraglacial lake	9	Cook and Quincey, 2015
11	$V = 60A - 6.28$	Worldwide	Moraine-dammed lake	42	Cook and Quincey, 2015
12	$V = 2.63e^A$	Worldwide	Ice-dammed lake	9	Cook and Quincey, 2015
13	$V = 37.3A^{1.47}$	Himalayas	Moraine-dammed lake	33	Khanal et al., 2015
14	$V = 52.2A^{1.18}$	Himalayas	Proglacial lake	6	Sharma et al., 2018
15	$V = 40A^2 + 5.06A$	Himalayas	Moraine-dammed lake	17	Patel et al., 2017
16	$V = 35.36A^{1.47}$	Central Asia	Moraine-dammed lake	32	Kapitsa et al., 2017
17	$V = 32.13A^{1.49}$	Himalayas	Ice-dammed lake, supraglacial lake	not mentioned	Miles et al., 2018
18	$V = 28.95A^{1.33}$	Worldwide	Moraine-dammed lake	93	Watson et al., 2018
19	$V = 35.46A^{1.4016}$	Himalayas	Supraglacial lake	24	Watson et al., 2018
19	$V = 41WA + 2A$	Cordillera Blanca, Peru	Moraine-dammed lake	120	Muñoz et al., 2020
20	$V = 37.36A^{1.41}$	Peruvian Andes	Various types	170	Wood et al., 2021
21	$V = 38.04A^{1.36}$	Peruvian Andes	Moraine-dammed lake	not mentioned	Wood et al., 2021
22	$V = 43.27A^{1.64}$	Peruvian Andes	Unclassified	not mentioned	Wood et al., 2021

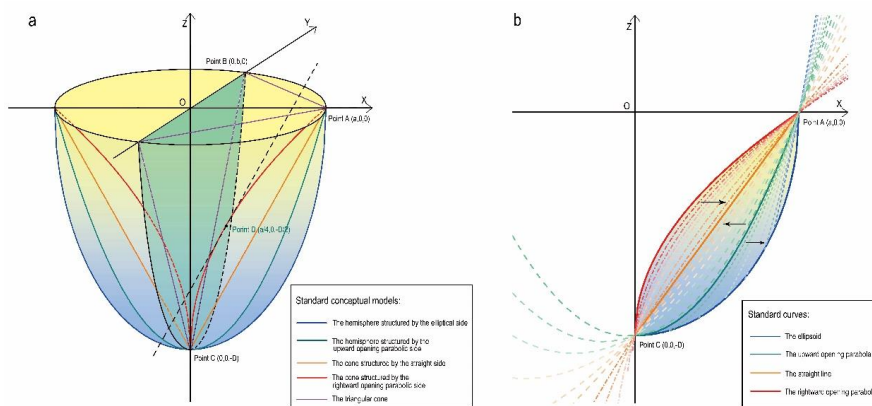
167

168



169

170 **Figure 2.** Relationships between maximum water depth and the area of glacial lakes were compiled in the present  
 171 study for the following lake types: (a) proglacial lake, (b) periglacial lake, (c) extraglacial lake, (d) supraglacial lake,  
 172 and (e) ice-dammed lake.

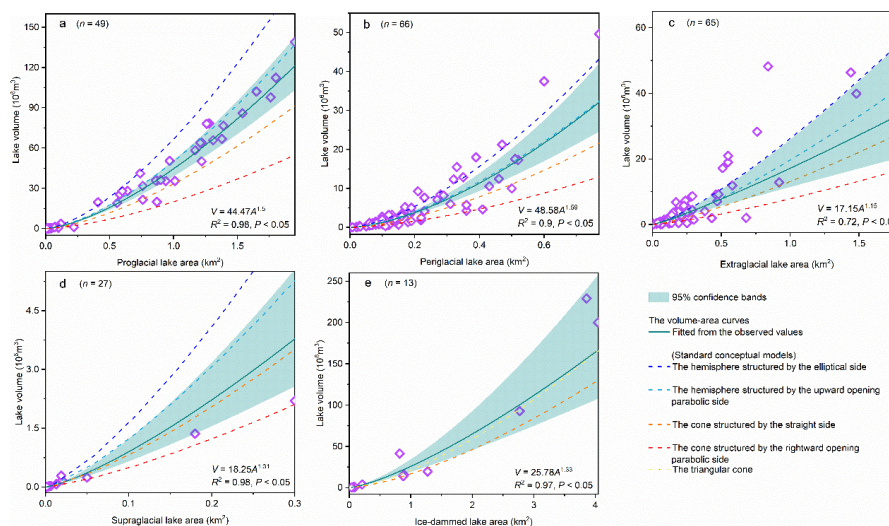


173

174 **Figure 3.** (a) Schematic diagram illustrates the shapes of the SCMs, namely the hemisphere structured by the  
 175 elliptical side/upward-opening parabolic side, the cone structured by the straight side/rightward-opening parabolic  
 176 side, the triangular cone, as well as their shapes when symmetrically divided matching the SCMs of the proglacial



177 lake. Here, A is the semi-long axis, B is the elliptical surface's semi-short axis, and D is the maximum water depth.  
 178 (b) Convergences of the general curves towards the standard curves in the X–O–Z quadrant in different orientations.



179  
 180 **Figure 4.** Relationships between the volume (V) and area (A) of glacial lakes were compiled in the present study for  
 181 the following lake types: (a) proglacial lake, (b) periglacial lake, (c) extraglacial lake, (d) supraglacial lake, and (e)  
 182 ice-dammed lake. The dotted lines indicate the volume curves of different standard conceptual models, which were  
 183 fitted by Eq. (3). The V–A curves of standard conceptual models of the proglacial lake type are half the normal  
 184 condition.

## 185 2.4 General conceptual model

186 The closest SCM likely does not represent the most appropriate conceptual model if a specific  
 187 glacial lake determines its parameters such as surface size, type, and volume. The SCM volume  
 188 curve is constant. However, the volume point of a specific glacial lake does not necessarily coincide  
 189 with the SCM volume curve. Thus, using the SCM directly to nest and interpolate a realistic glacial  
 190 lake bathymetric distribution would result in an initial over- or underestimation of the total lake



191 volume.

192 The SCMs can only help us comprehend the various glacial lake morphologies; they cannot be  
193 applied to estimate the glacial lake bathymetric distribution. We may conceive the measured volume  
194 points between the SCM volume curves as a result of the transition from one SCM to another. For  
195 instance, from the upward-opening parabolic line to the straight line, it is the standard parabolic line  
196 continuously approximating the straight line on the X–O–Z quadrant by moving downward and left  
197 (Fig. 3b). During the movement process, the rotated-out hemisphere is moving toward the cone  
198 structured by the straight side. We can capture these general conceptual models (GCMs) in this  
199 transition stage and make their volume consistent with the measured or estimated lake volume. This  
200 means we find a GCM that is more effective than the SCM in estimating the lake depth distribution.

201 Python programming was used to drive the standard curves' transition and parameter  
202 calculations. The theoretical description for the GCMs is presented in supplementary material 2. By  
203 relocating the standard curve's vertices and altering the opening size, it is simple to compute the  
204 transition of a standard upward/rightward-opening parabola to a straight line. The resultant general  
205 curves must pass through points A and C. The convergence to the standard elliptic curve from the  
206 standard upward-opening parabola is relatively complicated. If we move the vertices of the standard  
207 parabola to the right and downward, the maximum height of the produced GCM changes. We used  
208 a compound style here. When the second intersection of the moved general parabolic curve and the  
209 standard elliptic curve occurs (from right to left), the side of GCM starts to take the elliptic curve  
210 change. Additionally, the marginal SCMs should be employed when the measured volume is larger  
211 (smaller) than the largest (smallest) SCM volume.



## 212 **2.5 Nesting the actual glacial lake shapes**

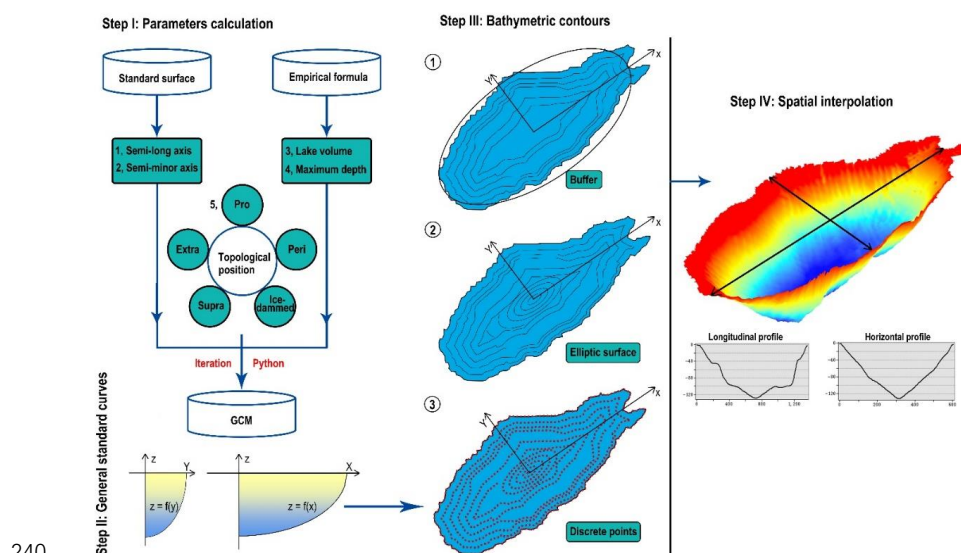
213       Once a given glacial lake's GCM has been established, the lake's bathymetric contours may be  
214 predicted in relation to actual conditions and parameters. Since the actual shape of the glacial lake  
215 surface is irregular, rather than the normal elliptic surface we used in the models, it was crucial to  
216 how the depth contours move inward based on the actual shape.

217       We tested two hypotheses. First, utilizing the lakeshore line to continually create buffers inward  
218 might depict the depth contours because the depth contours near the lakeshore were the consequence  
219 of ongoing indentation of the actual glacial lake surface outline inward. Second, at the 1/4 semi-  
220 long axis of the standard elliptic surface, the depth contours would become progressively blurred as  
221 the inward indentation continues, thus subsequently using the standard elliptic surface to start the  
222 inward indentation (Fig. 5). Importantly, these assumptions were supported by observations of  
223 hundreds of glacial lake bathymetric distribution cases worldwide. Some similarities exist between  
224 the bathymetric contours and the lakeshore shape, suggesting that the area near the lakeshore is  
225 possibly impacted by the slopes around the lake and/or other material sources. There are two  
226 explanations for this phenomenon: either the glacial lakes were continuously filled with exogenous  
227 debris and rocks, or the initial lake water level had risen and flooded part of the original slopes.

228       The 1/4 semi-long axis is the ending position where the glacial lake is not impacted by  
229 exogenous materials, as determined by our understanding of those SCMs. Most of the glacial lake  
230 SCMs were located closer to the cone, structured by the straight side of the hemisphere and the  
231 upward-opening parabolic side. It is inferred that the initial deepening of the glacial lake is not  
232 particularly large from the outer line to the center (compared to the semi-ellipsoid), indicating that



233 exogenous materials are likely to have impacted it. This situation is better understood when the lake  
 234 SCM is a cone structured by the rightward-opening parabolic side. Therefore, we hypothesized an  
 235 extreme circumstance in which a glacial lake starts to be significantly influenced by the lake's  
 236 surroundings' topography. In this case, the slope of the standard rightward-opening parabolic curve  
 237 is smaller than the slope of the standard straight line and closer to the ideal deepening state of the  
 238 lake basin when it is larger. This equal slope point is located at the 1/4 semi-long axis and represents  
 239 half of the maximum water depth.



240  
 241 **Figure 5.** The procedure illustrates the parameter calculation of GCMs and processes of creating buffers inward.  
 242 The water depths on the axes were calculated using the standard curves corresponding to the X and Y axes.

## 243 2.6 Sites for exhibiting and validating results

244 Three sets of bathymetry data were collected for the typical glacial lakes in the Himalayas,  
 245 Tibetan Plateau (Fig. 6). Cirenmaco and Jialongco, periglacial lakes, are located in the Poiqu River  
 246 basin (China-Nepal border). Both lakes experienced GLOFs in 1981 and 2002, causing severe



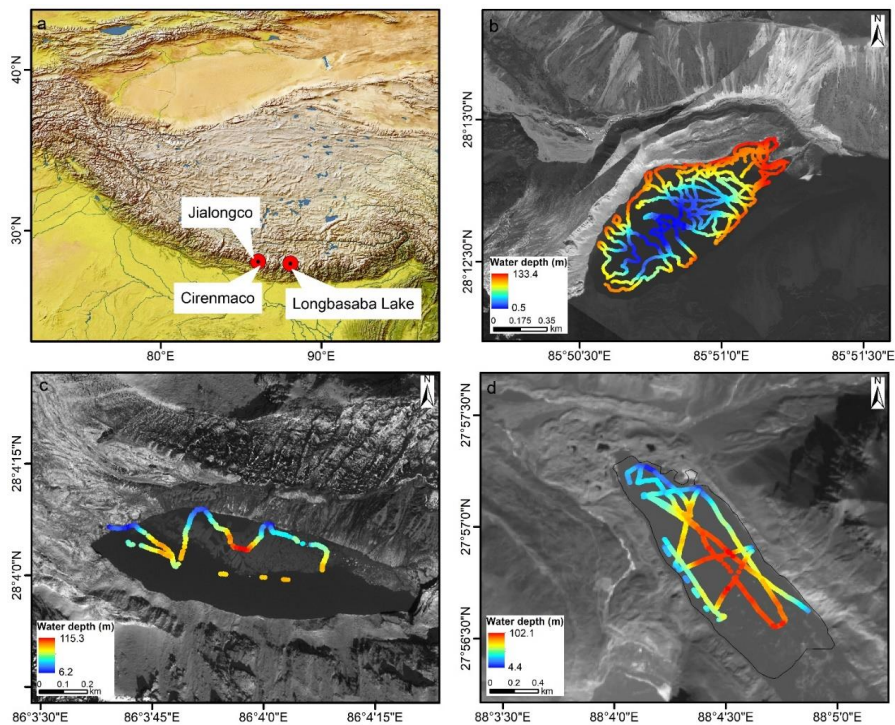
247 infrastructure losses and transboundary damages (Chen et al., 2013). The Longbasaba Lake at the  
248 China–India border is a benchmark proglacial lake that has been studied in detail for the glacial lake  
249 risks and dynamics of the lake-terminating glaciers (Yao et al., 2012; Wei et al., 2021). The  
250 topological position, total volume, maximum water depth, and semi-long/minor axis of the standard  
251 lake surface were crucial parameters in glacial lake bathymetric distribution modeling (Table 2).  
252 The three glacial lake bathymetric distributions were simulated according to the lake sizes in the  
253 survey year and eventually compared with the measured points of water depths to verify the  
254 feasibility and accuracy of our modeling method.

255 **Table 2.** The crucial modeling parameters of the three selected glacial lakes.

Name	Topological position	Survey year	Volume ( $10^6 \text{ m}^3$ )	Maximum water depth (m)	Semi-long axis (m)	Semi-minor axis (m)
Jialongco	peri	2020	37.5	133	757	314
Cirenmaco	peri	2012	18.0	115	549	185
Longbasaba Lake	pro	2009	64.0	102	1949	319

256





257

258 **Figure 6.** (a) Locations of Cirenmaco, Jialongco, and Longbasaba Lake, and (b, c, d) indications for their water  
259 depths along the bathymetric routes.

260

### 261 **3 Results**

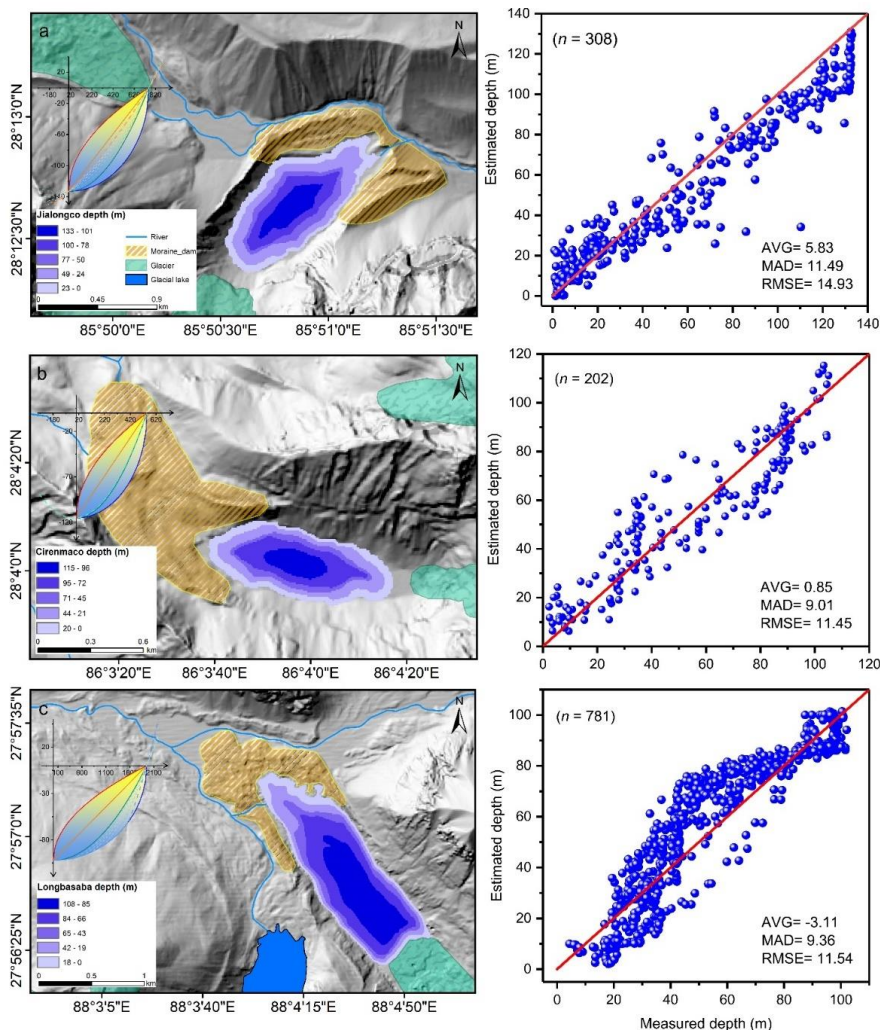
262 We present the SCMs for each type of glacial lake and demonstrate a procedure to identify the  
263 most compatible GCM for a specific glacial lake by equalizing the volume of both. This is the only  
264 (or first) model to simulate the bathymetric distribution of glacier lakes at present. The results  
265 indicate that the proglacial and periglacial lakes are relatively deep because their SCMs are closer  
266 to the hemisphere structured by the upward-opening parabolic side. The SCMs of the extraglacial  
267 and supraglacial lakes are closer to the cone structured by the straight side. As the ice-dammed lake,



268 their V–A fitting curve is more similar to the V–A curve of the triangular cone (Fig. 3). Hence, we  
269 recommend that the bathymetric distribution modeling for ice-dammed lakes proceeds directly  
270 using the standard triangular cone and is not further explored in this study.

271 We determined the optimal GCMs for the three exhibited glacial lakes. Following bathymetric  
272 distribution modeling results, the total volume of Jialongco was calculated to be  $33.1 \times 10^6 \text{ m}^3$   
273 ( $-11.7\%$ ) with a mean water depth of  $54.6 \text{ m}$  ( $-8.1\%$ ). Its GCM was closer to the cone structured  
274 by the straight side (Fig. 7a). The computed Cirenmaco total volume and mean depth of Cirenmaco  
275 were  $17.2 \times 10^6 \text{ m}^3$  ( $-4.4\%$ ) and  $51.7 \text{ m}$  ( $-6.9\%$ ), respectively. The Cirenmaco GCM had similarities  
276 with the hemisphere structured by the upward-opening parabolic side (Fig. 7b), meaning a more  
277 significant inward deepening rate than Jialongco. The proglacial lake, Longbasaba, was estimated  
278 to have a total volume of  $71.4 \times 10^6 \text{ m}^3$  ( $11.5\%$ ) and a mean depth of  $61.1 \text{ m}$  ( $22.2\%$ ). Its GCM was  
279 more resemblant to the semi-ellipsoid (Fig. 7c). Approximately  $\pm 10\%$  volume loss or increase was  
280 estimated in the process of nesting the general conceptual models to the actual glacial lake shapes.

281 The disparity between the area of the assumed standard ellipse surface and the actual lake  
282 surface likely caused the majority of the inaccuracy. The initial settings of glacial lake conceptual  
283 models and the algorithm's applicability were confirmed by comparison with the measured and  
284 estimated individual water depths. Between the estimated and measured water depths along the  
285 bathymetric routes, the average deviation, mean absolute deviation, and mean root square error for  
286 the three glacial lakes all described good consistency. Neither near the lakeshore nor the lake center  
287 do the estimates show intolerable dispersions.



288

289 **Figure 7.** Modeled glacial lake bathymetric distributions of the three selected glacial lakes. (a) Jialongco, (b)  
290 Cirenmaco, and (c) Longbasaba Lake. The average deviation (AVG), mean absolute deviation (MAD), and root  
291 mean square error (EMSE) were selected to depict the consistency between the simulated and measured individual  
292 water depths along the boat routes. The movements of the general curves from one standard curve to another are  
293 also indicated.

294



295 **4 Discussion**

296 **4.1 Glacial lake basin evolution**

297 Understanding the glacial lake evolution can help comprehend these idealized geometric  
298 shapes in theory. Most moraine- or bedrock-dammed lakes develop in depressions exposed by  
299 diminishing glaciers. The supraglacial lakes exist at the glacier snout, eventually facilitating the  
300 formation of proglacial and periglacial lakes (Carrivick and Tweed, 2013). As the three glacial lakes  
301 illustrated, our hypotheses explained the different rates of inward deepening with exogenous  
302 materials and boundary conditions impacting the glacial lakes. The glacier bedrock has been eroded  
303 and nudged during historical ice flowing, posing the excavation and growth of glacial lake basins.

304 Contemporary glaciers often have a certain thickness of debris at the snout. For example,  
305 approximately 1 m of debris was observed at the snout of the Urumqi Glacier No. 1, China  
306 (Echelmeyer et al., 1987) as the result of glacial erosion. The specific sites of continual eroding and  
307 nudging spawn overdeepenings and are considered potential glacial lakes (Linsbauer et al., 2016).  
308 Since the glacier velocity in the middle part is often larger than that of both sides, the erosion is  
309 stronger in the central line of the initial overdeepening. As glacier flowing continues, the shape of  
310 the overdeepening finally reaches equilibrium and is similar to a hemisphere, which is the SCM of  
311 the lake basin we assumed. After the overdeepenings are exposed, they can be filled by meltwater  
312 to form glacial lakes while also receiving material deposition, resulting in a gradual transition of the  
313 idealized geometric basin from a hemisphere to a cone. This conjecture can be inferred from the  
314 studies of overdeepenings on glacial beds, whereby the volume and surface area of these potential  
315 glacial lakes are also in accordance with the power-law relationship (Zhang et al., 2022).



## 316 **4.2 Applicability of the conceptual model**

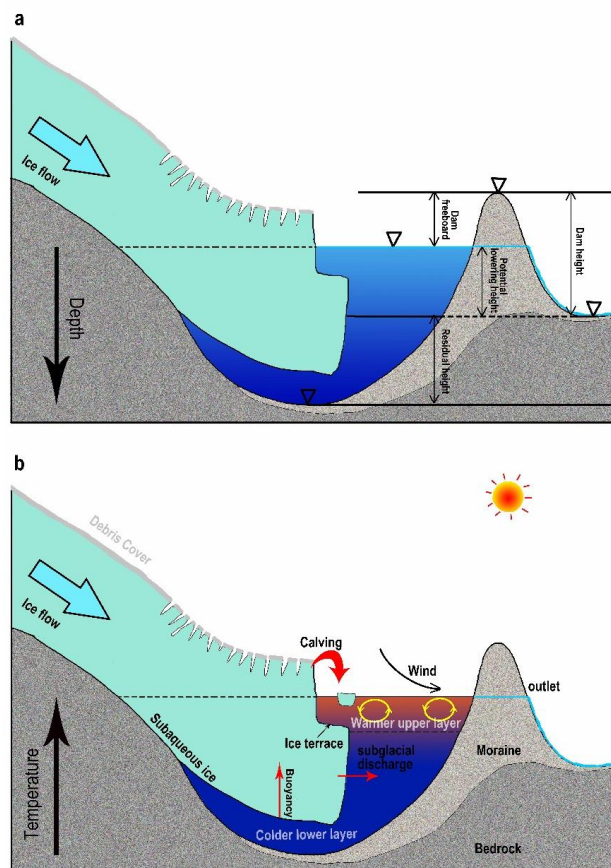
317 Our modeling theory is based on the observation of glacial lake bathymetric distribution  
318 characteristics. The fitted curves of glacial lake volume-area/maximum water depth were derived  
319 from the compiled inventory of 231 bathymetric data globally, and thus this modeling approach is  
320 applicable to most glacial lakes in mountain glaciers. The designed conceptual model is more  
321 suitable for those glacial lakes with typically lengthy shapes. They may be less applicable for very  
322 irregularly shaped glacial lakes, such as the ice-marginal lakes in the Greenland and Alaska region.  
323 Similarly, we had not collected any glacial lake bathymetry data in polar regions which causes non-  
324 applicability on supraglacial lakes over the Greenland/Antarctic Ice sheets. Although the simulated  
325 results were only validated in the Himalayan region due to the limitations of observation data, the  
326 comparison results of the measured and modeled depth values at different locations of the three  
327 glacial lakes reflect the rationality and reliability of our conceptual model. To our knowledge,  
328 roughly 80% of glacial lakes in the Tibetan Plateau and its surroundings can be modeled using this  
329 method.

330 In addition to the subjective and objective errors made during the modeling phase, there are  
331 several systematic defects in the algorithm itself. First, the total volume and maximum water depth  
332 are calculated using empirical equations, which may lead to significant deviations when modeling  
333 the bathymetric distribution of an arbitrarily selected glacial lake. In particular, the curves of D–A  
334 are not robust, with many discrete points appearing. This affects the modeling results. Therefore,  
335 rather than employing the curves based on global bathymetry statistics, fitting and using more  
336 accurate regionally empirical formulae to reveal local glacial lake features is encouraged.



337           Second, the estimated depth contours converge inward using the lake shoreline buffers first,  
338 followed by the elliptical surfaces. This process may effectively simulate the connections between  
339 a bathymetric distribution and glacial lake morphology. However, it is not essential. If the elliptical  
340 indentations are always inward relative to the elliptical surface, the modeling accuracy is also not  
341 affected significantly in theory.

342           Third, the deepest sites of supraglacial, periglacial, and extraglacial lakes have been considered  
343 to be in the lake center and near the glacier-lake interface for proglacial lakes and ice-dammed lakes.  
344 The developing proglacial lakes, however, are complex. Their deepest sites are constantly located  
345 near the glacier terminus before the deepest site of overdeepening is exposed, which is in accordance  
346 with our hypothesis. With the deepest sites developing more fully, they gradually shift toward the  
347 lake center. Our algorithm has not addressed these changes. In the future, the conceptual model  
348 requires optimization by learning with a number of measured bathymetry data. Furthermore, the  
349 present version of our algorithm relies on simple programming and semi-automated geospatial  
350 analysis tools processing. We will further develop this conceptual model to create an interface that  
351 can automatically process and lessen subjective errors.



352

353 **Figure 8.** The schematic diagrams illustrate (a) the potential maximum lowering height of the glacial lake water

354 level after drainage and (b) the interactions between the parent glacier and its terminating lake.

### 355 4.3 Applications in GLOF modeling

356 The applicability of a glacial lake bathymetric distribution has been addressed in this study;

357 one such application is in GLOF modeling. The results make two significant contributions to future

358 GLOF modeling: (i) accurately estimate the maximum potential outburst water volume of a glacial

359 lake by combining lake surface elevation, dam bottom elevation, and the optimal GCM; (ii) facilitate

360 coupling between the various GLOF processes in modeling (trigger—displacement wave—dam



361 breach—flood propagation). Many recent studies have documented reconstructing the historical  
362 GLOFs and simulating the future GLOFs from high outburst potential glacial lakes (Allen et al.,  
363 2015; Anacona et al., 2015b; Erokhin et al., 2017; Kougkoulos et al., 2018). The modeling precision  
364 is expected to improve significantly.

365 On the one hand, most prior studies replaced the potential maximum outburst volume with the  
366 total water volume because of the limitations of glacial lake bathymetric investigations (Zhang et  
367 al., 2021). Although this could present a maximized risk assessment, an inflated downstream  
368 exposure might raise excessive concerns among the authorities and the public regarding inadequate  
369 prevention and mitigation measures. As long as the dam's lowest elevation exceeds that of the  
370 glacial lake (potential lowering height is less than the maximum water depth), it could result in  
371 incomplete drainage (Fig. 8a).

372 On the other hand, due to the complicated phase transition in the chain process of GLOFs, a  
373 segmented simulation has been generally conducted. For instance, Rapid Mass Movement  
374 Simulation (RAMMS) can be used to simulate the impact of ice avalanches or landslides on glacial  
375 lakes (Frey et al. 2018; Sattar et al. 2021), and hydrological algorithms are used to calculate the  
376 displacement wave (Heller et al. 2009; Evers et al. 2019). Modeling software like IBER, HEC-RAS,  
377 or FLO-2D are employed to simulate downstream flood propagation (Alho and Aaltonen, 2008; Osti  
378 and Egashira, 2009; Schneider et al., 2014; Somos-Valenzuela et al., 2015; Maurer et al., 2020; Nie  
379 et al. 2020).

380 In contrast to a holistic simulation, such a segmented simulation approach undoubtedly causes  
381 poor articulation and increased uncertainty in different processes. With the recent scientific





382 developments, a newly developed three-phase flow model, r.avaflow (Mergili et al., 2017), started  
383 to be used to simulate GLOF propagations (Mergili et al., 2018, 2020) and can realize the whole  
384 hazard cascade modeling with a high performance (Zheng et al., 2021). Our study can provide much-  
385 needed glacial lake bathymetry data for such modeling to calculate the displacement wave in the  
386 lake surface and the water release process during dam erosion.

#### 387 **4.4 Potential developments of numerical or physical models**

388 The standardized glacial lake basin can facilitate other future model development related to  
389 glacial lakes and improve knowledge of how the proglacial lakes and lake-terminating glaciers  
390 interact. Carrivick et al. (2020) discussed six major challenges in constructing a numerical model  
391 of interactions between proglacial lakes and glaciers, which include the imperative for glacial lake  
392 bathymetry. The standardized shape implicates the design of the model's basic architecture.

393 Compared with the somewhat realistic glacier bed topography within the overdeepenings  
394 revealed by Ice Thickness Models, a standardized lake basin provides an alternative scheme. For a  
395 specific proglacial lake, its water level, water temperature, in/outflow, internal circulation, and  
396 interface with the glacier vary with glacier-lake dynamics and time, which are very complex  
397 processes (Sugiyama et al., 2016; Sutherland et al., 2020). Deep and large proglacial lakes are prone  
398 to water stratification due to warmer upper layers and colder lower layers of water because these  
399 freshwater terminating lakes currently have no evidence of active internal circulation (Haresign and  
400 Warren, 2005; Boyce et al., 2007). This stratification induces the subaqueous ice differential melting  
401 and ice terrace formation (Fig. 8b), impacting the glacier terminal calving regimes (Sugiyama et al.,  
402 2019; Mallalieu et al., 2020).



403 On the other hand, the dynamic characteristics of glacier snout, such as bed friction,  
404 longitudinal stress, and ice flow velocity, vary distinctively due to the presence of terminating lakes  
405 (Sugiyama et al., 2011; Liu et al., 2020). The knowledge and understanding of glacial lakes  
406 formation and evolution changes continually. The ultimate goal is to present these processes via  
407 computer numerical simulations. Yet, the idealized lake basin can facilitate calculating the mass and  
408 energy transport at the interface.

409

## 410 **5 Conclusion**

411 This study was conducted in response to a circumstance that field investigation was the only  
412 approach to obtain glacial lake bathymetry. The relationships of volume–area and maximum water  
413 depth–area of glacial lakes were reanalyzed via an inventory of the global glacial lake bathymetry  
414 data we compiled. The obtained curves were matched with a power-law relationship. Thus, the types  
415 of hemispheres or cones were determined as the conceptual models (idealized geometric shapes) of  
416 glacial lakes. The standard lake surface was assumed to be an ellipse.

417 Ten standard conceptual models were identified. The SCMs for the supraglacial, periglacial,  
418 and extraglacial lakes are the hemisphere structured by the elliptical side; the hemisphere structured  
419 by the upward-opening parabolic side; the cone structured by the straight side; and the cone  
420 structured by the rightward-opening parabolic side. The SCMs for the proglacial lakes were  
421 determined to be half of the aforementioned four SCMs. Two SCMs were considered for the ice-  
422 dammed lakes: the semi–cone structured by the straight side and the triangular cone. To depict the  
423 volume between the two SCMs, a general conceptual model was defined that represents the



424 transition from one SCM to another.

425         Several hypotheses are important in our algorithm to nest the actual glacial lake shapes from  
426 idealized conceptual models and interpolate glacial lake bathymetric distribution. First, the  
427 supraglacial, periglacial, and extraglacial lakes' deepest sites were assumed to be in the lake center,  
428 whereas the proglacial lakes and ice-dammed lakes' deepest sites were near the glacier-lake interface.  
429 Second, the effects of exogenous materials and boundary conditions were used to explain the  
430 different rates of inward deepening of glacial lakes. Three glacial lakes with measured bathymetry  
431 data were selected in the Himalaya region for comparison with the simulated bathymetric  
432 distributions. The results demonstrated good accuracy and applicability of our conceptual models  
433 in estimating lake bathymetry. Relatively high consistency was shown in the point-to-point  
434 comparisons of the measured and simulated water depths.

435         This study constructed the glacial lake bathymetric distribution model in first which is very  
436 rewarding for comprehending the evolution of glacial lakes. Moreover, the quality of GLOF  
437 modeling and risk assessment is also enhanced by our outlined general conceptual model. These  
438 standardized lake basins implicate the design of the model's basic architecture, which can  
439 potentially promote the development of future numerical or physical models of glacial lakes.

440

441 *Code availability.* The codes for calculating the functional equations of a general conceptual model  
442 in the coordinate axes are available on request.

443 *Data availability.* The observed bathymetric data of Jialongco and Longbasaba Lake were provided  
444 by Dr. Xiaojun Yao and Shanguan Donghui, respectively.



445 *Supplement.* The supplement related to this article is available online at:

446 *Author contributions.* TZ designed the study, compiled the data and drafted the manuscript. WW

447 and BA revised and edited the manuscript.

448 *Competing interests.* The authors declare that they have no conflict of interest.

449 *Financial support.* This study was supported by the Second Tibetan Plateau Scientific Expedition

450 and Research (STEP) Program (2019QZKK0208); the Strategic Priority Research Program of the

451 Chinese Academy of Sciences (XDA20100300); and the International Partnership Program of

452 Chinese Academy of Sciences (131C11KYSB20200029).

453

## 454 **References**

455 Aggarwal, S., Rai, S. C., Thakur, P. K., and Emmer, A.: Inventory and recently increasing GLOF susceptibility of  
456 glacial lakes in Sikkim, Eastern Himalaya, *Geomorphology*, 295, 39–54,  
457 <http://dx.doi.org/10.1016/j.geomorph.2017.06.014>, 2017.

458 Alho, P., and Aaltonen, J.: Comparing a 1D hydraulic model with a 2D hydraulic model for the simulation of extreme  
459 glacial outburst floods, *Hydrol. Process*, 22, 1537–1547. <http://dx.doi.org/10.1002/hyp.6692>, 2018.

460 Allen, S. K., Rastner, P., Arora, M., Huggel, C., and Stoffel, M. (2016). Lake outburst and debris flow disaster at  
461 Kedarnath, June 2013: hydrometeorological triggering and topographic predisposition, *Landslides*, 13, 1479–  
462 1491, <http://dx.doi.org/10.1007/s10346-015-0584-3>, 2015.

463 Anaconda, P. I., Mackintosh, A., Norton, K. P.: Hazardous processes and events from glacier and permafrost areas:  
464 lessons from the Chilean and Argentinean Andes, *Earth Surf. Process Landf.*, 40, 2–21,  
465 <http://dx.doi.org/10.1002/esp.3524>, 2015a.

466 Anaconda, P. I., Mackintosh, A., Norton, K.: Reconstruction of a glacial lake outburst flood (GLOF) in the Engano  
467 Valley, Chilean Patagonia: Lessons for GLOF risk management, *Sci. Total Environ.*, 527–528, 1–11,  
468 <http://dx.doi.org/10.1016/j.scitotenv.2015.04.096>, 2015b.

469 Bolch, T., Buchroithner, M. F., Peters, J., Pradhan, B., Buchroithner, M., and Blagoveshchensky, V.: Identification  
470 of glacier motion and potentially dangerous glacial lakes in the mt. Everest region/Nepal using spaceborne  
471 imagery, *Nat. Hazard Earth Syst.*, 8, 1329–1340, <http://dx.doi.org/10.1007/s11069-011-9860-2>, 2011.



- 472 Boyce, E. S., Motyka, R. J., and Truffer, M.: Flotation and retreat of a lake-calving terminus, Mendenhall Glacier,  
473 southeast Alaska, USA, *J. of Glaciol.*, 53, 211–224, <http://dx.doi.org/10.3189/172756507782202928>, 2007.
- 474 Carrivick, J. L., and Tweed, F. S.: Proglacial lakes: character, behaviour and geological importance, *Quat. Sci.*  
475 *Rev.*, 78, 34–52, <http://dx.doi.org/10.1016/j.quascirev.2013.07.028>, 2013.
- 476 Carrivick, J. L., and Tweed, F. S.: A global assessment of the societal impacts of glacier outburst floods, *Glob. Planet.*  
477 *Change*, 144, 1–16, <http://dx.doi.org/10.1016/j.gloplacha.2016.07.001>, 2016.
- 478 Carrivick, J. L., Tweed, F. S., Sutherland, J. L., and Mallalieu, J.: Toward numerical modeling of interactions between  
479 ice-marginal proglacial lakes and glaciers, *Front. Earth Sci.*, 500, <https://doi.org/10.3389/feart.2020.577068>,  
480 2020.
- 481 Chen, N. S., Hu, G. S., Deng, W., Khanal, N., Zhu, Y. H., and Han, D.: On the water hazards in the trans-boundary  
482 Kosi River basin, *Nat. Hazard Earth Syst. Sci.*, 13, 795–808, [http://dx.doi.org/10.1007/978-981-10-2890-8\\_17](http://dx.doi.org/10.1007/978-981-10-2890-8_17),  
483 2013.
- 484 Cook, S. J., Quincey, D. J.: Estimating the volume of Alpine glacial lakes, *Earth Surf. Dyn.*, 3, 559–575,  
485 <http://www.earth-surf-dynam.net/3/559/2015/doi:10.5194/esurf-3-559-2015>, 2015.
- 486 Drenkhan, F., Huggel, C., Guardamino, L., and Haerberli, W.: Managing risks and future options from new lakes in  
487 the deglaciating Andes of Peru: The example of the Vilcanota-Urubamba basin, *Sci. Total Environ.*, 665, 465–  
488 483, <https://doi.org/10.1016/j.scitotenv.2019.02.070>, 2019.
- 489 Echelmeyer, K., Wang Z. X.: Direct observation of basal sliding and deformation of basal drift at sub-freezing  
490 temperatures, *J. Glaciol.*, 33, 83–98. <http://dx.doi.org/10.3189/s0022143000005396>, 1987.
- 491 Emmer, A., and Vilímek, V.: New method for assessing the susceptibility of glacial lakes to outburst floods in the  
492 Cordillera Blanca, Peru, *Hydrol. Earth Syst. Sci.*, 18, 3461–3479, <http://www.hydrol-earth-syst-sci.net/18/3461/2014/doi:10.5194/hess-18-3461-2014>, 2014.
- 494 Emmer, A., Klimeš, J., Mergili, M., Vilímek, V. and Cochachin, A.: 882 lakes of the Cordillera Blanca: An inventory,  
495 classification, evolution and assessment of susceptibility to outburst floods, *Catena*, 147, 269–279,  
496 <http://dx.doi.org/10.1016/j.catena.2016.07.032>, 2016.
- 497 Erokhin, S. A., Zaginaev, V. V., Meleshko, A. A., Ruiz-Villanueva, V., Petrakov, D. A., Chernomorets, S. S.,  
498 Viskhadzhiyeva, K. S., Tutubalina, O. V., and Stoffel, M.: Debris flows triggered from non-stationary glacier  
499 lake outbursts: the case of the Teztor Lake complex (Northern Tian Shan, Kyrgyzstan), *Landslides*, 15, 83–98,  
500 <http://dx.doi.org/10.1007/s10346-017-0862-3>, 2018.
- 501 Evans, S. G.: The maximum discharge of outburst floods caused by the breaching of man-made and natural dams,  
502 *Can. Geotech. J.*, 23(3), 385–387, <http://dx.doi.org/10.1139/t87-062>, 1986.
- 503 Evers F. M., Heller, V., Fuchs, H., Hager, W. H., and Boes, R. M.: Landslide-generated Impulse Waves in Reservoirs:



- 504 Basics and Computation, VAW-Mitteilungen, 254, 2019.
- 505 Falatkova, K., Šobr, M., Neureiter, A., Schöner, W., Janský, B., Häusler, H., Engel, Z., and Beneš, V.: Development  
506 of proglacial lakes and evaluation of related outburst susceptibility at the Adygine ice-debris complex, northern  
507 Tien Shan, Earth Surf. Dyn., 7, 301–320, <https://doi.org/10.5194/esurf-7-301-2019>, 2019.
- 508 Frey, H., Huggel, C., Chisolm, R. E., Baer, P., McArdell, B., Cochachin, A., and Portocarrero, C.: Multi-source  
509 glacial lake outburst flood hazard assessment and mapping for Huaraz, Cordillera Blanca, Peru, Front. Earth  
510 Sci., 6, 210. <https://doi.org/10.3389/feart.2018.00210>, 2018.
- 511 Fujita, K., Sakai, A., Takenaka, S., Nuimura, T., Surazakov, A. B., Sawagaki, T., and Yamanokuchi, T.: Potential  
512 flood volume of Himalayan glacial lakes, Nat. Hazard Earth Syst. Sci., 13, 1827–1839, [http://www.nat-hazards-](http://www.nat-hazards-earth-syst-sci.net/13/1827/2013/doi:10.5194/nhess-13-1827-2013)  
513 [earth-syst-sci.net/13/1827/2013/doi:10.5194/nhess-13-1827-2013](http://www.nat-hazards-earth-syst-sci.net/13/1827/2013/doi:10.5194/nhess-13-1827-2013), 2013.
- 514 Haresign, E., and Warren, C. R.: Melt rates at calving termini: a study at Glaciar León, Chilean Patagonia, Geological  
515 Society, London, Special Publications, 242, 99–109, <http://dx.doi.org/10.1144/GSL.SP.2005.242.01.09>, 2005.
- 516 Heller, V., Hager, W. H., Minor, H. E.: Landslide Generated Impulse Waves in Reservoirs, Zurich: Mitteilungen  
517 Versuchsanstalt für Wasserbau, Hydrologie und Glaziologie (VAW), ETH Zürich, 2019.
- 518 Huggel, C., Kääb, A., Haeberli, W., Haeberli, W., Teysseire, P., and Paul, F.: Remote sensing based assessment of  
519 hazards from glacier lake outbursts: a case study in the Swiss Alps, Can. Geotech. J., 39, 316–330,  
520 <http://dx.doi.org/10.1139/t01-099>, 2002.
- 521 Hugonnet, R., McNabb, R., Berthier, E., Menounos, B., Nuth, C., Girod, L., Farinotti, D., Huss, M., Dussailant, I.,  
522 Brun, F., and Kääb, A.: Accelerated global glacier mass loss in the early twenty-first century, Nature, 592, 726–  
523 731, <https://doi.org/10.1038/s41586-021-03436-z>, 2021.
- 524 Kapitsa, V., Shahgedanova, M., Machguth, H., Severskiy, I., and Medeu, A.: Assessment of evolution and risks of  
525 glacial lake outbursts in the Djungarskiy Alatau, Central Asia, using Landsat imagery and glacier bed  
526 topography modelling, Nat. Hazard Earth Syst. Sci., 17, 1837–1856, [https://doi.org/10.5194/nhess-17-1837-](https://doi.org/10.5194/nhess-17-1837-2017)  
527 [2017](https://doi.org/10.5194/nhess-17-1837-2017), 2017.
- 528 Khanal, N. R., Hu, J. M., and Mool, P.: Glacial lake outburst flood risk in the Poiqu/Bhote Koshi/Sun Koshi river  
529 basin in the Central Himalayas, Mt. Res. Dev., 35, 351–364, [http://dx.doi.org/10.1659/MRD-JOURNAL-D-15-](http://dx.doi.org/10.1659/MRD-JOURNAL-D-15-00009)  
530 [00009](http://dx.doi.org/10.1659/MRD-JOURNAL-D-15-00009), 2015.
- 531 Kougkoulos, I., Cook, S. J., Edwards, L. A., Clarke, L. J., Symeonakis, E., Dortch, J. M., and Nesbitt, K.: Modelling  
532 glacial lake outburst flood impacts in the Bolivian Andes, Nat. Hazard, 94, 1415–1438,  
533 <https://doi.org/10.1007/s11069-018-3486-6>, 2018.
- 534 Li, D., Shangquan, D. H., Wang, X., Ding, Y. J., Su, P. C., Liu, R. L., and Wang, M. X.: Expansion and hazard risk  
535 assessment of glacial lake Jialong Co in the central Himalayas by using an unmanned surface vessel and remote  
536 sensing, Sci. Total Environ., 784, <https://doi.org/10.1016/j.scitotenv.2021.147249>, 2021.



- 537 Linsbauer, A., Frey, H., Haeblerli, W., Machguth, H., Azam, M. F., and Allen, S.: Modelling glacier-bed  
538 overdeepenings and possible future lakes for the glaciers in the Himalaya—Karakoram region, *Ann. Glaciol.*,  
539 57, 119–130, <http://dx.doi.org/10.3189/2016AoG71A627>, 2016.
- 540 Liu, Q., Mayer, C., Wang, X., Nie, Y., Wu, K. P., Wei, J. F., and Liu, S. Y.: Interannual flow dynamics driven by  
541 frontal retreat of a lake-terminating glacier in the Chinese Central Himalaya, *Earth Planet. Sci. Lett.*, 546,  
542 116450, <https://doi.org/10.1016/j.epsl.2020.116450>, 2020.
- 543 Lliboutry, L., Armao, B. M., Pautre, A., and Schneider, B.: Glaciological problems set by the control of dangerous  
544 lakes in Cordillera Blanca, Peru. I. Historical failures of morainic dams, their causes and prevention, *J. Glaciol.*,  
545 18, 239–254, <http://dx.doi.org/10.1017/S002214300002133X>, 1977.
- 546 Loriaux, T., Casassa, G.: Evolution of glacial lakes from the Northern Patagonia Icefield and terrestrial water storage  
547 in a sea-level rise context, *Glob. Planet. Change*, 102, 33–40, <http://dx.doi.org/10.1016/j.gloplacha.2012.12.012>,  
548 2013.
- 549 Ma, J. S., Song, C. Q., Wang, Y. J.: Spatially and Temporally Resolved Monitoring of Glacial Lake Changes in Alps  
550 During the Recent Two Decades, *Front. Earth Sci.*, 9, <https://doi.org/10.3389/feart.2021.723386>, 2021.
- 551 Mallalieu, J., Carrivick, J. L., Quincey, D. J., and Smith, M. W.: Calving seasonality associated with melt -  
552 undercutting and lake ice cover, *Geophys. Res. Lett.*, 47, e2019GL086561,  
553 <https://doi.org/10.1029/2019GL086561>, 2020.
- 554 Maurer, J. M., Schaefer, J. M., Russell, J. B., Rupper, S., Wangdi, N., Putnam, A. E., and Young, N.: Seismic  
555 observations, numerical modeling, and geomorphic analysis of a glacier lake outburst flood in the Himalayas,  
556 *Sci. Adv.*, 6, eaba3645, <http://dx.doi.org/10.1126/sciadv.aba3645>, 2020.
- 557 Mergili, M., Fischer, J. T., Krenn, J., Pudasaini, S. P.: r. avaflow v1, an advanced open-source computational  
558 framework for the propagation and interaction of two-phase mass flows, *Geosci. Model Develop.*, 10, 553–569,  
559 <http://dx.doi.org/10.5194/gmd-10-553-2017>, 2017.
- 560 Mergili, M., Emmer, A., Juricova, A., Cochachin, A., Fischer, G. T., Huggel, C., and Pudasaini, S. P.: How well can  
561 we simulate complex hydro-geomorphic process chains? The 2012 multi-lake outburst flood in the Santa Cruz  
562 Valley (Cordillera Blanca, Peru), *Earth Surf. Process. Landf.*, 431373–1389, <http://dx.doi.org/10.1002/esp.4318>,  
563 2018.
- 564 Mergili M, Pudasaini SP, Emmer A, Fischer, G. T., Cochachin, A., Frey, H.: Reconstruction of the 1941 GLOF  
565 process chain at Lake Palcacocha (Cordillera Blanca, Peru), *Hydrol. Earth Syst. Sci.*, 24, 93–114,  
566 <https://doi.org/10.5194/hess-24-93-2020>, 2020.
- 567 Miles, E. S., Watson, C. S., Brun, F., Berthier, E., Esteves, M., Quincey, D. J., Miles, K. E., Hubbard, B., and Wagnon,  
568 P.: Glacial and geomorphic effects of a supraglacial lake drainage and outburst event, Everest region, Nepal  
569 Himalaya, *The Cryosphere*, 12, 3891–3905, <https://doi.org/10.5194/tc-12-3891-2018>, 2018.



- 570 Muñoz, R., Huggel, C., Frey, H., Cochachin, A., and Haeberli, W.: Glacial lake depth and volume estimation based  
571 on a large bathymetric dataset from the Cordillera Blanca, Peru, *Earth Surf. Process. Landf.*,  
572 <http://dx.doi.org/10.1002/esp.4826>, 2020.
- 573 Nie, Y., Liu, Q., Wang, J. D., Zhang, Y. L., Sheng, Y. W., and Liu, S. Y.: An inventory of historical glacial lake  
574 outburst floods in the Himalayas based on remote sensing observations and geomorphological analysis,  
575 *Geomorphology*, 308, 91–106, <https://doi.org/10.1016/j.geomorph.2018.02.002>, 2018.
- 576 Nie, Y., Liu, W., Liu, Q., Hu, X., and Westoby, M. J.: Reconstructing the Chongbaxia Tsho glacial lake outburst flood  
577 in the Eastern Himalaya: Evolution, process and impacts, *Geomorphology*, 370, 107393,  
578 <https://doi.org/10.1016/j.geomorph.2020.107393>, 2020.
- 579 O'Connor, J. E., Hardison III, J. H., Costa, J. E.: *Debris Flows from Failures of Neoglacial-Age Moraine Dams in  
580 the Three Sisters and Mount Jefferson Wilderness Areas, Oregon*, 105 pp, 2001.
- 581 Osti, R., and Egashira, S.: Hydrodynamic characteristics of the Tam Pokhari glacial lake outburst flood in the Mt.  
582 Everest region, Nepal, *Hydrol. Process.*, 23, 2943–2955, <http://dx.doi.org/10.1002/hyp.7405>, 2009.
- 583 Patel, L. K., Sharma, P., Laluraj, C. M., Thamban, M., Singh, A., and Ravindra, R.: A geospatial analysis of Samudra  
584 Tapu and Gepang Gath glacial lakes in the Chandra Basin, Western Himalaya, *Nat. Hazard*, 86, 1275–1290,  
585 <https://link.springer.com/article/10.1007/s11069-017-2743-4>, 2017.
- 586 Petrov, M. A., Sabitov, T. Y., Tomashevskaya, I. G., Glazirin, G. E., Chernomorets, S. S., Savernyuk, E. A.,  
587 Tutubalina, O. V., Petrakov, D. A., Sokolov, L. S., Dokukin, M. D., Mountrakis, G., Ruiz-Villanueva, V., and  
588 Stoffel, M.: Glacial lake inventory and lake outburst potential in Uzbekistan, *Sci. Total Environ.*, 592, 228–242,  
589 <http://dx.doi.org/10.1016/j.scitotenv.2017.03.068>, 2017.
- 590 Richardson, S. D., Reynolds, J. M.: An overview of glacial hazards in the Himalayas, *Quat. Int.*, 65–6, 31–47,  
591 [http://dx.doi.org/10.1016/S1040-6182\(99\)00035-X](http://dx.doi.org/10.1016/S1040-6182(99)00035-X), 2000.
- 592 Sakai, A.: Glacial lakes in the Himalayas: a review on formation and expansion processes, *Glob. Environ. Res.*, 16,  
593 23–30, 2012.
- 594 Sattar, A., Haritashya, U. K., Kargel, J. S., Leonard, G. J., Shugar, D. H., and Chase, D. V.: Modeling lake outburst  
595 and downstream hazard assessment of the Lower Barun Glacial Lake, Nepal Himalaya, *J. Hydrol.*, 598, 126208.  
596 <https://doi.org/10.1016/j.jhydrol.2021.126208>, 2021.
- 597 Schneider, D., Huggel, C., Cochachin, A., Guillén, S., and García, J.: Mapping hazards from glacier lake outburst  
598 floods based on modelling of process cascades at Lake 513, Carhuaz, Peru, *Adv. Geosci.*, 35, 145–155,  
599 <http://dx.doi.org/10.5194/adgeo-35-145-2014>, 2014.
- 600 Sharma, R. K., Pradhan, P., Sharma, N. P., and Shrestha, D. G.: Remote sensing and in situ-based assessment of  
601 rapidly growing South Lhonak glacial lake in eastern Himalaya, India, *Nat. Hazard*, 93, 393–409,  
602 <https://doi.org/10.1007/s11069-018-3305-0>, 2018.





- 603 Shugar, D. H., Burr, A., Haritashya, U. K., Kargel, J. S., Watson, C. S., Kennedy, M. C., Bevington, A. R., Betts, R.  
604 A., Harrison, S., and Stratman, K.: Rapid worldwide growth of glacial lakes since 1990, *Nat. Clim. Change*,  
605 10, 939–945, <https://doi.org/10.1038/s41558-020-0855-4>, 2020.
- 606 Somos-Valenzuela, M. A., McKinney, D. C., Byers, A. C., Rounce, D. R., Portocarrero, C., and Lamsal, D.:  
607 Assessing downstream flood impacts due to a potential GLOF from Imja Tsho in Nepal, *Hydrol. Earth Syst.*  
608 *Sci.*, 19, 1401–1412, <http://dx.doi.org/10.5194/hess-19-1401-2015>, 2015.
- 609 Sugiyama, S., Skvarca, P., Naito, N., Enomoto, H., Tsutaki, S., Tone, K., Marinsek, S., and Aniya, M.: Ice speed of a  
610 calving glacier modulated by small fluctuations in basal water pressure, *Nat. Geosci.*, 4, 597–600,  
611 <http://dx.doi.org/10.1038/ngeo1218>, 2011.
- 612 Sugiyama, S., Minowa, M., Sakakibara, D., Skvarca, P., Sawagaki, T., Ohashi, Y., Naito, N., and Chikita, K.: Thermal  
613 structure of proglacial lakes in Patagonia, *J. Geophys. Res.: Earth Surf.*, 121, 2270–2286,  
614 <http://dx.doi.org/10.1002/2016JF004084>, 2016.
- 615 Sugiyama, S., Minowa, M., and Schaefer, M.: Underwater ice terrace observed at the front of Glaciar Grey, a  
616 freshwater calving glacier in Patagonia, *Geophys. Res. Lett.*, 46, 2602–2609,  
617 <http://dx.doi.org/10.1029/2018GL081441>, 2019.
- 618 Sugiyama, S., Minowa, M., Fukamachi, Y., Hata, S., Yamamoto, Y., Sauter, T., Schneider, C., and Schaefer, M.:  
619 Subglacial discharge controls seasonal variations in the thermal structure of a glacial lake in Patagonia, *Nat.*  
620 *Commun.*, 12, 1–9, <https://doi.org/10.1038/s41467-021-26578-0>, 2021.
- 621 Sutherland, J. L., Carrivick, J. L., Gandy, N., Shulmeister, J., Quincey, D. J., and Cornford, S. L.: Proglacial lakes  
622 control glacier geometry and behavior during recession, *Geophys. Res. Lett.*, 47, e2020GL088865,  
623 <https://doi.org/10.1029/2020GL088865>, 2020.
- 624 Veh, G., Korup, O., and Walz, A.: Hazard from Himalayan glacier lake outburst floods, *PNAS*, 117, 907–912,  
625 <https://www.pnas.org/cgi/doi/10.1073/pnas.1914898117>, 2020.
- 626 Wang, X., Liu, S. Y., Ding, Y. J., Guo, W. Q., Jiang, Z. L., Lin, J., and Han, Y.: An approach for estimating the breach  
627 probabilities of moraine-dammed lakes in the Chinese Himalayas using remote-sensing data, *Nat. Hazard Earth*  
628 *Syst. Sci.*, 12, 3109–3122, <http://dx.doi.org/10.5194/nhess-12-3109-2012>, 2012.
- 629 Wang, X., Guo, X. Y., Yang C. D., Liu, Q. H., Wei, J. F., Zhang, Y., Liu, S. Y., Zhang, Y. L., Jiang, Z. L., and Tang,  
630 Z. G.: Glacial lake inventory of high-mountain Asia in 1990 and 2018 derived from Landsat images, *Earth Syst.*  
631 *Sci. Data*, 12, 2169–2182, <https://doi.org/10.5194/essd-12-2169-2020>, 2020.
- 632 Wang, W. C., Gao, Y., Anaconda, P. I., Lei, Y. B., Xiang, Y., Zhang, G. Q., Li, S. H., and Lu, A. X.: Integrated hazard  
633 assessment of Cirenmaco glacial lake in Zhangzangbo valley, Central Himalayas, *Geomorphology*, 306, 292–  
634 305, <http://dx.doi.org/10.1016/j.geomorph.2015.08.013>, 2018.
- 635 Watson, C. S., Quincey, D. J., Carrivick, J. L., Smith, M. W., Rowan, A. V., and Richardson, R.: Heterogeneous



- 636 water storage and thermal regime of supraglacial ponds on debris-covered glaciers, *Earth Surf. Process. Landf.*,  
637 43, 229–241, <http://dx.doi.org/10.1002/esp.4236>, 2018.
- 638 Wei, J. F., Liu, S. Y., Wang, X., Zhang, Y., Jiang, Z. L., Wu, K. P., Zhang, Z., and Zhang, T.: Longbasaba Glacier  
639 recession and contribution to its proglacial lake volume between 1988 and 2018, *J. Glaciol.*, 67, 473–484,  
640 <https://doi.org/10.1017/jog.2020.119>, 2021.
- 641 Westoby, M. J., Glasser, N. F., Brasington, J., Hambrey, M. J., Quincey, D. J., and Reynolds, J. M.: Modelling  
642 outburst floods from moraine-dammed glacial lakes, *Earth-Sci. Rev.*, 134, 137–159,  
643 <http://dx.doi.org/10.1016/j.earscirev.2014.03.009>, 2014.
- 644 Wood, J. L., Harrison, S., Wilson, R., Emmer, A., Yarleque, C., Glasser, N. F., Torres, J. C., Caballero, A., Araujo, J.,  
645 Bennett, G. L., Diaz-Moreno, A., Garay, D., Jara, H., Poma, C., Reynolds, J. M., Riveros, C. A., Romero, E.,  
646 Shannon, S., Tinoco, T., Turpo, E., and Villafane, H.: Contemporary glacial lakes in the Peruvian Andes, *Glob.*  
647 *Planet. Change*, 204, 103574, <https://doi.org/10.1016/j.gloplacha.2021.103574>, 2021.
- 648 Yao, T. D., Thompson, L., Yang, W., Yu, W. S., Gao, Y., Guo, X. J., Yang, X. X., Duan, K. Q., Zhao, H. B., Xu, B.,  
649 Q., Pu, J. C., Lu, A. X., Xiang, Y., Kalltel, D. B., and Joswiak, D.: Different glacier status with atmospheric  
650 circulations in Tibetan Plateau and surroundings, *Nat. Clim. Change*, 2, 663–667,  
651 <http://www.nature.com/doi/10.1038/nclimate1580>, 2012.
- 652 Yao, T. D., Xue, Y. K., Chen, D. L., Chen, F. H., Thompson, L., Cui, P., Koike, T., K.-M. Lau, W., Lettenmaier, D.,  
653 Mosbrugger, V., Zhang, R. H., Xu, B. Q., Dozier, J., Gillespie, T., Gu, Y., Kang, S. C., Piao, S. L., Sugimoto,  
654 S., Ueno, K., Wang, L., Wang, W. C., Zhang, F., Sheng, Y. W., Guo, W. D., Ailikun, Yang, X. X., Ma, Y. M.,  
655 Shen, S. S. P., Su, Z. B., Chen, F., Liang, S. L., Liu, Y. M., Singh, V. P., Yang, K., Yang, D. Q., Zhao, X. Q.,  
656 Qian, Y., Zhang, Y., and Li, Q.: Recent third pole's rapid warming accompanies cryospheric melt and water  
657 cycle intensification and interactions between monsoon and environment: Multidisciplinary approach with  
658 observations, modeling, and analysis, *B. Am. Meteorol. Soc.*, 100, 423–444, [https://doi.org/10.1175/BAMS-D-](https://doi.org/10.1175/BAMS-D-17-0057.1)  
659 [17-0057.1](https://doi.org/10.1175/BAMS-D-17-0057.1), 2019.
- 660 Yao, X. J., Liu, S. Y., Sun, M. P., Wei, J. F., and Guo, W. Q.: Volume calculation and analysis of the changes in  
661 moraine-dammed lakes in the north Himalaya: a case study of Longbasaba lake, *J. Glaciol.*, 58, 753–760,  
662 <http://dx.doi.org/10.3189/2012JoG11J048>, 2012.
- 663 Yao, X. J., Liu, S. Y., Han, L., Sun, M. P., and Zhao, L. L.: Definition and classification system of glacial lake for  
664 inventory and hazards study, *J. Geogr. Sci.*, 28, 193–205, <https://doi.org/10.1007/s11442-018-1467-z>, 2018.
- 665 Zemp, M., Huss, M., Thibert, E., McNabb, R., Huber, J., Barandun, M., Machguth, H., Nussbaumer, S. U., Gärtner-  
666 roer, I., Thomson, L., Paul, F., Maussion, F., Kutuzov, S., and Cogley, J. G.: Global glacier mass changes and  
667 their contributions to sea-level rise from 1961 to 2016, *Nature*, 568, 382–386, [https://doi.org/10.1038/s41586-](https://doi.org/10.1038/s41586-019-1071-0)  
668 [019-1071-0](https://doi.org/10.1038/s41586-019-1071-0), 2019.
- 669 Zhang, G. Q., Yao, T. D., Xie, H. J., Wang, W. C., and Yang, Wei.: An inventory of glacial lakes in the Third Pole  
670 region and their changes in response to global warming, *Glob. Planet. Change*, 131, 148–157,



- 671 <http://dx.doi.org/10.1016/j.gloplacha.2015.05.013>, 2015.
- 672 Zhang, T. G., Wang, W. C., Gao, T. G., and An, B. S.: Simulation and Assessment of Future Glacial Lake Outburst  
673 Floods in the Poiqu River Basin, Central Himalayas, *Water*, 13, <https://doi.org/10.3390/w13101376>, 2021.
- 674 Zhang, T. G., Wang, W. C., An, B. S., Gao, T. G., and Yao, T. D.: Ice thickness and morphological analysis reveal  
675 the future glacial lake distribution and formation probability in the Tibetan Plateau and its surroundings, *Glob.*  
676 *Planet. Change*, 216, 103923, <https://doi.org/10.1016/j.gloplacha.2022.103923>, 2022.
- 677 Zheng, G. X., Mergili, M., Emmer, A., Allen, S., Bao, A. M., Guo, H., and Stoffel, M.: The 2020 glacial lake outburst  
678 flood at Jinwucuo, Tibet: causes, impacts, and implications for hazard and risk assessment, *The Cryosphere*, 15,  
679 3159–3180, <https://doi.org/10.5194/tc-15-3159-2021>, 2021.